BULGARIAN ACADEMY OF SCIENCES

SPACE RESEARCH IN BULGARIA, 1

*Sofia · 1978*

# Fault Structures Obtained by Geological Interpretation of Space Images

*H. B. Spiridonov, V. S. Djepa-Petrova*

New trends in studying various natural phenomena and objects appear within the development of aero- and space methods of Earth investigations through outer space. Particularly great are the possibilities for the Earth sciences of geology, geomorphology, soil studies, hydrology, and the like. Space images processing provides for the accumulation of enormous quantities of statistical material which broadens our knowledge in the field of Earth sciences. Particularly great are the prospects revealed by the statistical processing of fault structures obtained by a visual method of geological interpretation of space images.

This paper uses space multizonal images provided by the American technological satellite ERTS-1 for the purpose of statistical processing of fault structures. The photographs were obtained in four spectral ranges: 0.5—0.6, 0.6—0.7, 0.7—0.8, and 0.8—1 $\mu$m, i. e. in the visible and the near-infrared regions of the spectra. The geographical coordinates of the photographic centre are: N 41°42/E 026°03; N 41°40/E 026°05. The space photograph comprises a surface of $S=33502$ sq. km. It embraces the South-Eastern part of the Bulgarian territory, the Eastern Rhodope Mountains included, as well as most of Western and Eastern Thrace, which are part of Greece and Turkey.

The Eastern Rhodope block, which is the subject of the geological interpretation, is part of the Rhodope Median Massif. Four structural complexes participate in its tectonic configuration, namely: Archaen, Proterozoic, Caledono-Hercynian and Alpine. They form analogous structural plans [2]. The Eastern Rhodope morphostructural block has been the theatre of intense tectonic manifestations, mostly of a hereditary nature [2]. The different lithostratigraphical complexes are affected by multiple faults, in which the sequential structural decomposition of the massif is reflected.

All the tectonic disturbances have been separated irrespective of the corresponding structural plans, during the interpretation of the space photographs. The fault disturbances have been mapped (Fig. 1) on the basis of

the geological fault structures interpreted (mainly on channels 5 and 7, with wavelengths 0.6—0.7 and 0.8—1.1 $\mu$m). The map obtained was compared with the available tectonic, geological, neotectonic, geomorphological, soil and seismo-tectonic maps. Analogous Greek and Turkish maps were also

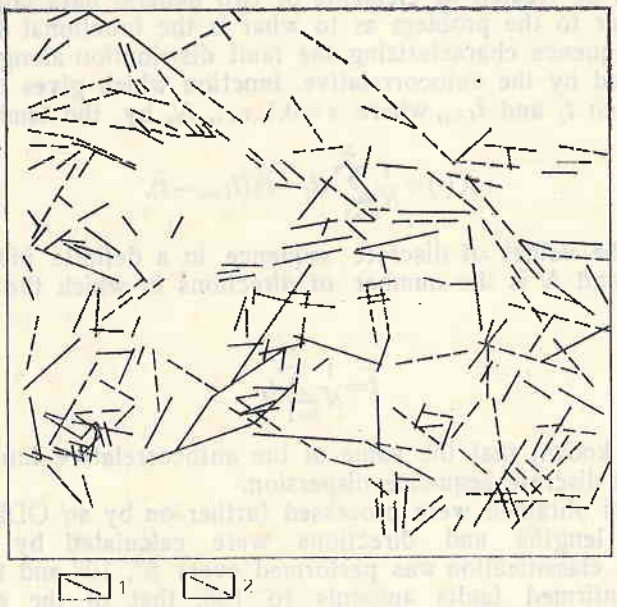


Fig. 1. Map of the fault structures obtained by the geological interpretation of the space images
1 — confirmed faults; 2 — suggested faults

used. Most of the tectonic structures, interpreted on the space images, confirmed the already known fault zones and faults. In addition, new structures unknown to the geological maps were identified. Together with the definite selection of most fault structures, a considerable number of them had provoked certain doubts. That is why these structures were divided conventionally into two categories: a) faults definitely identified on the space photographs, and b) suggested faults not definitely discerned on the space photographs. On the other hand, the space images embrace territories of neighbouring countries for which we are not in possession of detailed cartographical geological materials. This fact also contributed to adopting the decision for differentiating between the two fault categories.

The two fault structure categories — confirmed and suggested — obtained from the interpretation of the space multizonal photographs, were used for statistical processing with the specialized electronic system of automated digital recording for photogrammetric and cartographic information.

The set obtained with coordinates of the two fault-structure categories can be used further on for computer processing. For that purpose the essential indicators which characterize the multitude of faults are determined by the direction ($d_i$) and length ($l_i$) of the fault, where:

(1) $$d_i = \text{arctg}\,[(Y_{2i}-Y_{1i})/(X_{2i}-X_{1i})],$$

(2) $$l_i = \sqrt{(X_{2i}-X_{1i})^2+(Y_{2i}-Y_{1i})^2},$$

For the purposes of mathematical statistics, direction ($d_i$) and fault length ($l_i$) can be treated as elements of two general data populations.

The answer to the problem as to what is the functional dependence in the discrete sequence characterizing the fault distribution along the direction can be obtained by the autocorrelative function which gives the statistical relation between $t_i$ and $t_{i+\tau}$, where $\tau = 0.1, \ldots, N$, by the familiar formula:

(3) $$K(\tau) = \frac{1}{N}\sum_{i=1}^{N}(t_i-\bar{t})(t_{i+\tau}-\bar{t}),$$

where $t_i$ are the values of discrete sequence in a definite interval at fault classification, and $N$ is the number of directions in which the classification is performed.

(4) $$\bar{t} = \frac{1}{N}\sum_{i=1}^{N} t_i.$$

It is well known that the value of the autocorrelative function at $\tau = 0$ determines the discrete sequence dispersion.

The results obtained were processed further on by an ODRA computer. All the fault lengths and directions were calculated by formulae (1) and (2). A fault classification was performed every 5°, 10° and 15°. The total sum of the confirmed faults amounts to 165, that of the assumed ones being 80. Some additional data for computer processing are given in Table 1.

Table 1

| Faults | Number $n_i$ | Summary length/km $L$ | Maximum length/km $l_{max}$ | Minimum length/km $l_{min}$ | Density $\varrho = \frac{L}{S}$ [km$^{-1}$] |
|---|---|---|---|---|---|
| Confirmed | 165 | 1845.71 | 42.57 | 4.13 | 0.055081 |
| Suggested | 80 | 1261.88 | 37.75 | 4.98 | 0.03487 |

The classification results and the fault structure distribution are shown on histograms and fault rose (Figs. 2, 3). Both the histograms and the fault structure rose have been worked out at every 5°. The classification and the distributon of the two fault types have been effected in the range from 0° to 180°.

If we analyze thoroughly the fault distribution at intervals of 5° in the range indicated for the confirmed ones, and for the suggested faults — by histograms and the rose, we shall find considerable saturation (tips of the histograms) in the following directions: 0°, 25°, 40°, 50°, 90°, 105°, 125° and 175°. An interesting fault concentration may be observed in the North-Eastern quadrant in the range between 10° and 60° both for the confirmed and for the suggested faults. A constant fault background is present here and its tips are outlined in directions of 10°, 25°, 40°, 50°. The highest concentration for the faults suggested is in the same quadrant in a direction of 20°.

A particularly big saturation of faults is found in the interval from 90° to 95° and the concentration maximum is attained at 90°. If compared to (1) there would be almost full coincidence both along the amplitude of scattering (here it is of about 15°) and in the fault concentration in the

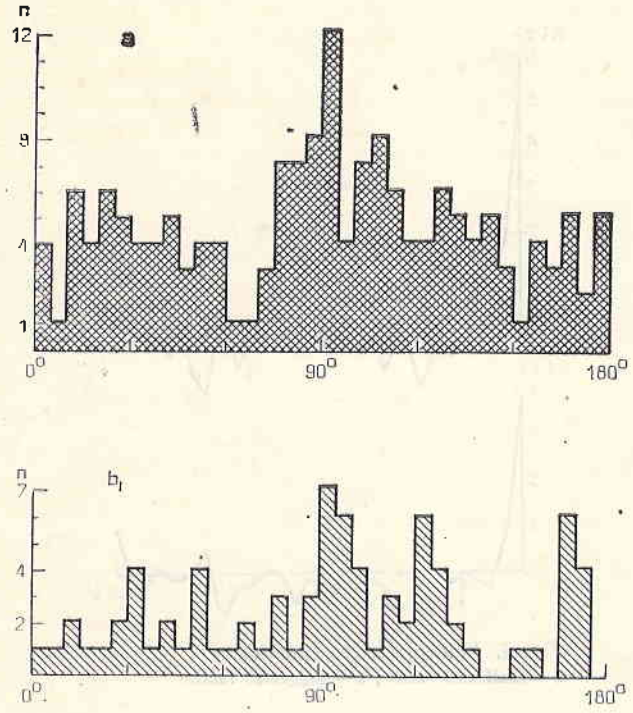


Fig. 2. Histograms :
a — confirmed faults ; b — suggested faults

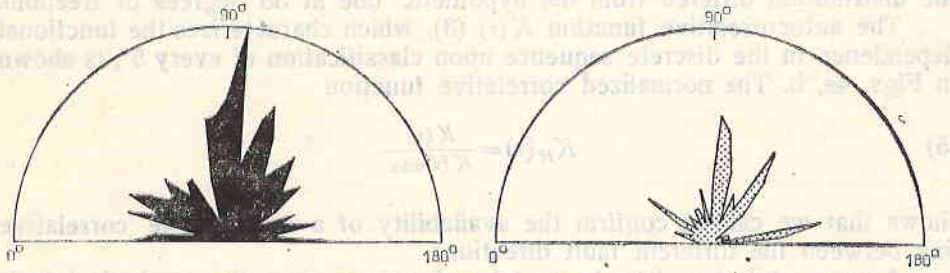


Fig. 3. Rose of the fault structures :
a — confirmed ; b — suggested

East-Western direction. This conclusion relates to both confirmed and suggested fault structures.

As far as the remaining interval concentrations in the North-Western quadrant are concerned, they completely correspond to the main fault structure with directions of 120°—130° and 150°—170° (1).

One basic problem arises here, namely: the determination of the specific distribution of the faults examined and the respective verification with the help of experimental data available. The histograms worked out (Fig. 2a, b) show mixed distribution. The verification of the uniform distribution

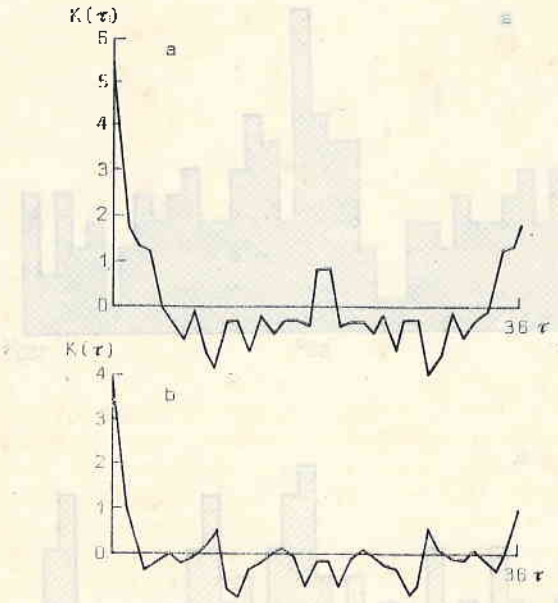


Fig. 4. Autocorrelative function:
a — confirmed faults ; b — suggested faults

availability was performed according to the $X_i$-square criterion (3) which had shown that with a probability higher than 0.995 we could confirm that the distribution differed from the hypothetic one at 35 degrees of freedom.

The autocorrelative function $K(\tau)$ (3), which characterizes the functional dependence in the discrete sequence upon classification at every 5°, is shown in Figs. 4a, b. The normalized correlative function

$$K_H(\tau)=\frac{K(\tau)}{K(\tau)_{max}} \tag{5}$$

shows that we cannot confirm the availability of a considerable correlative link between the different fault directions.

A successful step has been taken by processing the geological fault structures obtained by the visual method of interpretation of the multizonal space images of the South-Eastern Bulgarian territory. Such a processing has not been carried out until now. A comparison with (1) shows that the interpreted fault structures reflect correctly the total distribution of the fault systems in the Eastern half of the Balkan Peninsula. This fact proves once again that the suggested program of processing fault disturbances has been correctly worked out and is being successfully interpreted.

## References

1. Бончев, Е. Проблеми на българската тектоника. С., Техника, 1971.
2. Йовчев, И., А. Атанасов и др. Тектонски строеж на България, С., Техника, 1971.
3. Румшисткий, Л. С. Математическая обработка результатов эксперимента, М., Наука, 1971.
4. Spiridonov, H. B., D. Stoychev, M. Katskov. Results from the geological interpretation of space images of the East Rhodope mountains. — In: COSPAR, Varna, 1975.

## Разломные структуры, полученные при геологическом дешифрировании космических изображений

*Х. Б. Спиридонов, В. С. Джепа-Петрова*

(Резюме)

В результате визуального структурного дешифрирования многозональных космических изображений, охватывающих Восточные Родопы, выделяются линейные разломные структуры. На основе этих структур составлена карта разломных нарушений. Полученные линейные структуры подразделяются на две категории: а) достоверно отдешифрированные разломы, и б) предполагаемые разломы. Эти две категории разломов используются дальше для статистической обработки специализированной электронной системой автоматической цифровой регистрации фотограмметрической и картографической информации. Распределение разломных структур исследуется методами математической статистики.